NUCL SCI TECH (2021) 32:82
https://doi.org/10.1007/s41365-021-00915-w

Discrimination of neutrons and gamma rays in plastic scintillator based on pulse-coupled neural network

Hao-Ran Liu[1] · Yu-Xin Cheng[1] · Zhuo Zuo[1,2] · Tian-Tian Sun[1] · Kai-Min Wang[1]

Received: 19 April 2021 / Revised: 17 May 2021 / Accepted: 22 May 2021 / Published online: 5 August 2021

Abstract Neutron and gamma ray pulse signal discrimination technology is an essential part of many modern scientific fields, such as biology, geology, radiation imaging, and nuclear medicine. Neutrons are always accompanied by gamma rays due to their unique penetration characteristic; thus, the development of n-γ discrimination methods is especially crucial. In the present study, a novel n-γdiscrimination method is proposed that implements a pulse-coupled neural network for n-γ discrimination. In addition, experiments were conducted on the pulse signals detected by an EJ299-33 plastic scintillator, which is especially suitable for n-γ discrimination. The proposed method was compared to three other discrimination methods, including the back-propagation neural network (BPNN), the fractal spectrum method, and the charge comparison method, with respect to two aspects: (i) the figure of merit (*FoM*) and (ii) discrimination time.

The experimental results showed that the pulse-coupled neural network (PCNN) has a 26.49% improvement in *FoM*-value compared to the charge comparison method, a 72.80% improvement compared to the BPNN, a 66.24% improvement compared to the fractal spectrum method, and the second-fastest discrimination time of 2.22 s. In conclusion, the PCNN treats the input signal as a whole for analysis and processing, imparting it with an excellent anti-noise effect and the ability to process the dynamic information contained in a pulse signal.

Keywords Pulse-coupled neural network · Charge comparison · Back-propagation neural network · Fractal spectrum · n-γ discrimination

1 Introduction

In the past 50 years, neutron detection technology has become highly crucial in many areas, such as irradiation facilities [1], reactors [2], national defense [3], biology [4], geology [5], medical science [6], and deep-space exploration [7]. Because of the unique interaction between neutrons and the surrounding environment, neutrons are commonly accompanied by gamma rays. However, most radiation detectors used to detect neutrons are also sensitive to gamma rays, which makes n-γ discrimination especially important. In 1979, Brooks et al. [8] found that neutrons and gamma rays generated different pulse shapes when they interacted with organic detectors. Based on this difference between neutrons and gamma rays, pulse shape discrimination (PSD) has been studied [9, 10], many novel detectors with excellent performance have been developed [11, 12], and the feasibility of plastic scintillators for PSD applications has been studied [13–15]. Various discrimination methods and discussions of their performance have been introduced and Liu et al. presented a fractal spectrum method in 2016 [16], which has the advantages of anti-noise and high discrimination but requires a very long discrimination time. In 2021, Zuo and Liu et al. compared the performances of three different discrimination methods

This work was supported by the Key Science and Technology projects of Leshan (No. 19SZD117) and the Sichuan Science and Technology Program (No. 2021JDRC0108).

✉ Zhuo Zuo
690870641@qq.com

[1] The Engineering & Technical College of Chengdu University of Technology, Leshan 614000, China

[2] Southwestern Institute of Physics, Chengdu 610225, China

implemented by four different filtering methods [17]; the intelligent discrimination method they used was the conventional back-propagation neural network (BPNN), which requires the training and prediction sets to be highly similar and processes the dynamic information poorly [18].

Generally, all of the commonly used n-γ discrimination methods mentioned above can be categorized into three categories: time-domain, frequency-domain, and intelligent methods. Although the discrimination time of the time-domain methods is relatively short, their discrimination performances are not satisfactory. In addition, regarding the frequency-domain and intelligent methods, although these discrimination methods generally tend to outperform time-domain methods, most require a significant amount of matrix operations, i.e., the algorithm implementation could be relatively cumbersome and time-consuming, which is not conducive to real-time online analysis. These problems raise the question of whether it is possible to find an n-γ discrimination method that is capable of processing the dynamic information contained in the pulse signals, similar to the frequency-domain and intelligent methods while having low computational difficulty and maintaining its time consumption at the same level as the time-domain methods.

To solve this problem, we present a novel n-γ discrimination method, which is based on a pulse-coupled neural network (PCNN). Experiments were conducted to verify the performance of the proposed method, in which it was compared with the BPNN method, fractal spectrum method, and charge comparison method, with respect to the figure of merit (*FoM*) and discrimination time. To retrieve the data from the n-γ superposed field, a plastic scintillator (EJ299-33) and a digital oscilloscope were used, which was set with a sampling rate of 1 GS/s, a bandwidth of 200 MHz, and a trigger threshold of 500 mV. The pulse duration was 160 ns, respecting the Shanon criteria, and the bandwidth did not bury the useful signal [19]. The experimental results showed that the proposed method significantly outperformed the others, with an outstanding *FoM*-value and short discrimination time consumption.

The remainder of this paper is organized as follows: the fundamentals of our proposed method and the other three discrimination methods are presented in Sect. 2. The evaluation criteria of n-γ discrimination performance are proposed in Sect. 3. The discrimination results of the different methods are compared and discussed in Sect. 4. The conclusions of the work are presented in Sect. 5.

2 Fundamentals of discrimination methods

2.1 Pulse-coupled neural network

2.1.1 Origin and mathematical expression

The pulse-coupled neural network (PCNN) was introduced by Eckhorn and Reitboeck et al. in 1990 [20], which works similarly to real biological neurons, does not require cumbersome work to train the neural network before using it, and, hence, does not require the tested data to be highly similar to the trained data. Based on the neurophysiological findings of the cat's primary visual cortex [21, 22], they developed a neural network whose central novel principle was abandoning the conventional receptive field and instead introducing a secondary receptive field, the linking field. The integrated input of the aforementioned linking field has an internal cellular circuit, which is capable of modulating the primary feeding receptive field input, influencing the generation of pulse bursts. For a signal fed to the PCNN, which has multiple sampling points—usually, an image [23, 24] —the unique character of the linking field makes it possible to capture the dynamic properties contained in the signal and retrieve the inherent relationships between neighboring sampling points, which is especially crucial for processing signals whose dynamic information is as important as, if not more important than, the information of each sampling point.

The model of the PCNN incorporates the accepted, modulation, and pulse generator domains. The accepted domain has two components: feedback input (FI) and link input (LI), which together determine the potential of a neuron. When the potential of a neuron exceeds its dynamic threshold, it is considered activated. The mathematical formulas of the PCNN are as follows [25]:

$$\boldsymbol{F}_{ij}[n] = e^{-\alpha_{\mathrm{F}}}\boldsymbol{F}_{ij}[n-1] + V_{\mathrm{F}}\sum_{kl}\boldsymbol{M}_{ijkl}\boldsymbol{Y}_{kl}[n-1] + \boldsymbol{S}_{ij}, \quad (1)$$

$$\boldsymbol{L}_{ij}[n] = e^{-\alpha_{\mathrm{L}}}\boldsymbol{L}_{ij}[n-1] + V_{\mathrm{L}}\sum_{kl}\boldsymbol{M}_{ijkl}\boldsymbol{Y}_{kl}[n-1], \quad (2)$$

$$\boldsymbol{U}_{ij}[n] = \boldsymbol{F}_{ij}[n]\{1 + \beta\boldsymbol{L}_{ij}[n]\}, \quad (3)$$

$$\boldsymbol{Y}_{ij}[n] = \begin{cases} 1, \boldsymbol{U}_{ij}[n] > \boldsymbol{\theta}_{ij}[n] \\ 0, \text{otherwise} \end{cases}, \quad (4)$$

$$\theta_{ij}[n] = e^{-\alpha_{\theta}}\theta_{ij}[n-1] + V_{\theta}\boldsymbol{Y}_{ij}[n-1], \quad (5)$$

where $\boldsymbol{F}_{ij}$ and $\boldsymbol{L}_{ij}$ denote the FI and LI of (i,j), respectively, and coordinate (k,l) represents one of the neighboring neurons of (i,j); n is the iteration count; α_{F} and α_{L} represent the decay times of FI and LI, respectively; V_{F} and V_{L} denote the amplification coefficients of FI and LI, respectively; $\boldsymbol{M}$ is the connection weight matrix, which represents the extent of influence that central neurons received from

surrounding neurons; $\boldsymbol{S}_{ij}$ denotes the external input; β is a coefficient influencing the weight of FI and LI in internal activity threshold $\boldsymbol{U}_{ij}$; $\boldsymbol{\theta}_{ij}$ represents the dynamic threshold, and $\boldsymbol{Y}$ is the timing pulse sequence defined by $\boldsymbol{U}_{ij}$ and $\boldsymbol{\theta}_{ij}$; V_θ and α_θ denote the amplification coefficient and decay time of the dynamic threshold $\boldsymbol{\theta}_{ij}$, respectively. Note that the connections of the FI should be slower than those of the LI.

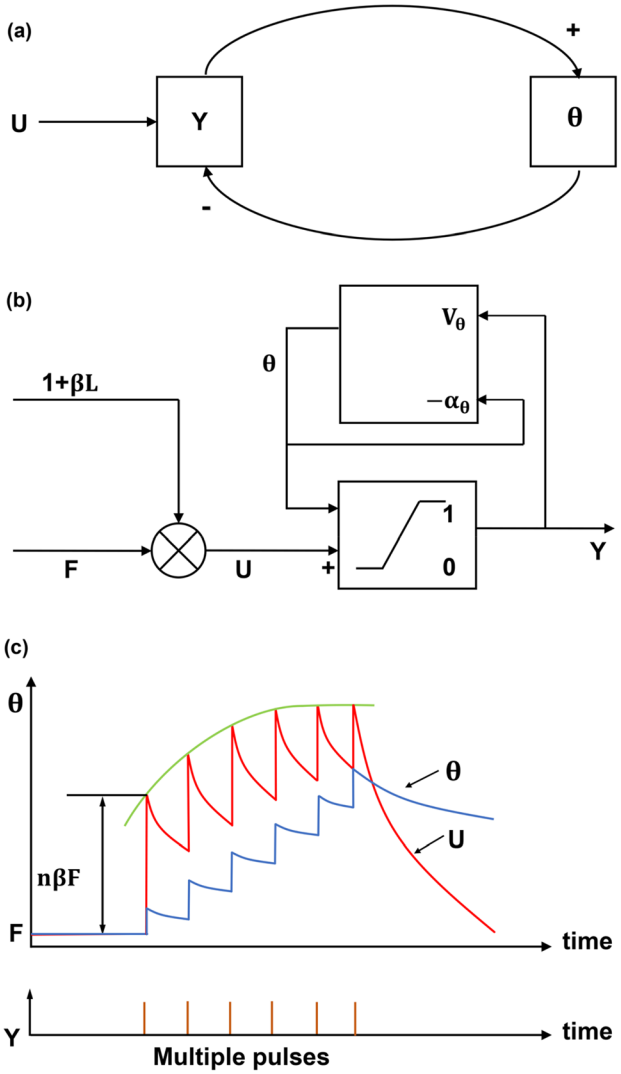

Fig. 1 (Color online) Schematic of the pulse-coupled neural network. **a** The relationship between $\boldsymbol{U}_{ij}$, $\boldsymbol{Y}$, and $\boldsymbol{\theta}_{ij}$. The internal activity threshold $\boldsymbol{U}_{ij}$ influences the timing pulse sequence $\boldsymbol{Y}$ and $\boldsymbol{Y}$ can further influence the dynamic threshold $\boldsymbol{\theta}_{ij}$; in turn, the changing dynamic threshold $\boldsymbol{\theta}_{ij}$ influences the state of the timing pulse sequence $\boldsymbol{Y}$. **b** The basic PCNN model. **c** The ignition situation of a neuron stimulated by multiple pulses. The internal activity threshold $\boldsymbol{U}_{ij}$ (or could be seen as the total input) and the dynamic threshold $\boldsymbol{\theta}_{ij}$ are simultaneously augmented by the multiple pulses (external input $\boldsymbol{S}_{ij}$). After stimulation via multiple pulses, the growth rate of $\boldsymbol{U}_{ij}$ begins to slow while that of $\boldsymbol{\theta}_{ij}$ remains, indicating that $\boldsymbol{\theta}_{ij}$ will eventually exceed $\boldsymbol{U}_{ij}$ and reset occurs

Intuitively, as shown in Fig. 1a, b, the internal activity threshold $\boldsymbol{U}_{ij}$ has a direct influence on the timing pulse sequence $\boldsymbol{Y}$ and $\boldsymbol{Y}$ can further influence the dynamic threshold $\boldsymbol{\theta}_{ij}$. Meanwhile, the change in the dynamic threshold $\boldsymbol{\theta}_{ij}$ influences the state of the timing pulse sequence $\boldsymbol{Y}$ because $\boldsymbol{Y}$ is defined by $\boldsymbol{U}_{ij}$ and $\boldsymbol{\theta}_{ij}$ together [26]. Regarding the ignition of a group of closely connected neurons, as shown in Fig. 1c, the internal activity threshold $\boldsymbol{U}_{ij}$ (or could be seen as the total input) and the dynamic threshold $\boldsymbol{\theta}_{ij}$ are simultaneously augmented by multiple pulses (external input $\boldsymbol{S}_{ij}$). After the stimulation of multiple pulses, the growth rate of $\boldsymbol{U}_{ij}$ begins to slow down while that of $\boldsymbol{\theta}_{ij}$ remains, which means that $\boldsymbol{\theta}_{ij}$ will eventually exceed $\boldsymbol{U}_{ij}$ and reset occurs. For each neuron, the number of times $\boldsymbol{U}_{ij}$ is greater than $\boldsymbol{\theta}_{ij}$ after stimulation by multiple pulses is defined as the ignition time, which is the value of the corresponding location of this neuron in the ignition map.

2.1.2 *Implementation on* n-γ *discrimination*

PCNN has a tremendous number of applications in image processing [26] but has never been used in the PSD field. Similar to the information contained in an image, the information contained in a pulse signal also has dynamic properties, which are essential to the discrimination process. The distinguished performance of the PCNN in processing dynamic information enables a computer to capture the dynamic characteristics of pulse signals and perform outstanding n-γ discrimination. Specifically, the major difference between neutron and gamma ray signals is in the falling edge and delayed fluorescence and the detection process of this difference does not only concern the amplitude of each sampling point of the falling edge and afterglow effect peak but is also related to the changing rate of the amplitudes in these locations, which is the aforementioned dynamic information one wants to capture, used to discriminate neutron and gamma ray signals.

When the PCNN is applied in neutron and gamma ray signal processing, the connection weight matrix $\boldsymbol{M}$ is a one-dimensional vector because the pulse signals of neutrons and gamma rays are one-dimensional. After implementing the PCNN on a pulse signal, an ignition map was obtained, i.e., a matrix with the same dimensions as the original signal. By summing up part of the ignition map that contains the information of a signal's peak and falling edge, the neutrons and gamma rays can be discriminated. Notice that, unlike other commonly used neural networks, the PCNN requires no training process before the discrimination process, making its computational complexity and time consumption much less than other conventional neural networks.

As shown in Fig. 3, the difference in the falling edge of neutrons and gamma rays is well detected by PCNN, exhibiting significant differences in the ignition maps of the n-γ signals. For the pulse signal of the gamma ray, the ignition times in the part of the falling edge decrease very quickly, which is attributed to the fast decay time of gamma ray pulse signals. Conversely, the declining speed of the ignition times in the part of the falling edge is noticeably slower for the neutron signals than that of the gamma ray pulses and the ignition times surge again when it comes to the part of delayed fluorescence. Consequently, by summing the ignition times of the partial ignition map that incorporates the rising edge, falling edge, and delayed fluorescence, the n-γ pulse signals could be well discriminated, granted that the sum of ignition times of neutron signals is distinctly larger than that of gamma ray signals.

2.2 Back-propagation neural network

2.2.1 Model and mathematical expression

The back-propagation neural network (BPNN) is a product of artificial intelligence research based on the back-propagation algorithm, which is capable of learning from the examples fed to it [27]. Specifically, adapting the connection weights of the hidden neurons of the BPNN can provide an accurate approximation of the relationship between the training set and corresponding results; sometimes, even the aforementioned relationship is nonlinear [28]. With regard to the BPNN, the mathematical relationships between the inputs and outputs are not specified and the learning process has two steps: forward propagation of the signal and backward propagation of error. Specifically, when the output of the BPNN differentiates from the expected output, defined by the training set, the backward propagation stage begins to adjust the inherent relationships of the hidden node. Mathematically, the hidden node output model and output node output model are denoted as follows:

$$\boldsymbol{O}_j = h\left(\sum \boldsymbol{W}_{ij} \times \boldsymbol{X}_i - q_j\right), \tag{6}$$

$$\boldsymbol{Y}_k = h\left(\sum \boldsymbol{T}_{jk} \times \boldsymbol{O}_j - q_k\right), \tag{7}$$

where $\boldsymbol{X}_i$ denotes the input of the BPNN, $\boldsymbol{O}_j$ represents the output of the hidden node, $\boldsymbol{Y}_k$ denotes the output of the BPNN, h is a nonlinear function, $\boldsymbol{W}_{ij}$ and $\boldsymbol{T}_{jk}$ are weight matrices that are adjusted during backward propagation, and q represents the neural unit threshold.

2.2.2 Implementation on n-γ discrimination

In recent decades, back-propagation neural networks have been fully developed to address many civil engineering problems. The final objective of applying n-γ discrimination [29, 30] is to determine the difference between neutron and gamma ray pulse signals, by which an inherent relationship between a pulse signal and its category can be generalized and further used to discriminate the n-γ pulse signals fed to the BPNN in the future. To realize the aforementioned aim, the BPNN needs to be trained first using two sets of already well-discriminated neutron and gamma ray pulse signals. In this training step, the BPNN tries to categorize the received pulse signals (the input patterns), with the recursive adjustment aided by the category results of each pulse signal (the output patterns). When the neural network has completed the training step, it can be used to process the test set and discriminate the pulse signals.

However, there are a few drawbacks of n-γ discrimination based on BPNN. The training and test sets need to be highly similar and hence these sets cannot use different filtering methods and the pulse signals of these two sets need to be retrieved from the same radiation detection device and come from the same radiation source, with the same average energy. These disadvantages restrict the general application of BPNN for n-γ discrimination.

2.3 Fractal spectrum

The fractal spectrum method discriminates n-γ signals using fractal dimensions, which are the power spectra of signals [16]. Specifically, the spectrum of a signal needs to first be calculated and then the frequency of this signal and its spectrum should be presented logarithmically, retrieving an approximate linear relationship between the aforementioned operation results. Finally, a linear regression analysis is implemented to obtain regression coefficients, which can be further used to discriminate the n-γ signals. The mathematical interpretation of the fractal spectrum method is defined as:

$$\boldsymbol{F}_{\mathrm{D}}(k) = \sum_{j=1}^{N} \boldsymbol{D}(j) w_N^{(J-1)(K-1)}, \tag{8}$$

$$w_N = e^{(-2\pi i)/N}, \tag{9}$$

$$\boldsymbol{P}_{\mathrm{SS}} = \frac{\left|\boldsymbol{F}_{\mathrm{D}}(k)\right|^2}{N}, \tag{10}$$

$$\boldsymbol{G}(w) = \boldsymbol{G}(w_0)\left(\frac{w}{w_0}\right)^{-\alpha}, \tag{11}$$

where $\boldsymbol{D}$ is the input data, N is the calculation length of the Fourier transform, $\boldsymbol{F}_{\mathrm{D}}$ is the data processed by the discrete Fourier transform, and $\boldsymbol{P}_{\mathrm{ss}}$ represents the power spectrum. Based on Eqs. (8), (9), and (10), the power spectral density function can be calculated. Then, the logarithm of this function is taken and further fitted by formula (11), where $\boldsymbol{G}(w)$ denotes the power spectral density of the signal, w_0 is the reference space frequency, w represents the spatial frequency, and $\boldsymbol{G}(w_0)$ denotes the signal conversion coefficient. Finally, the fractal dimension is defined as follows:

$$Dim = 2.5 - \alpha. \tag{12}$$

2.4 Charge comparison

The charge comparison method [31] has become one of the most commonly used n-γ discrimination methods, which has a fine n-γ discrimination performance and consumes little time for simultaneous discrimination processing. With regard to its internal principle, owing to the different interaction characteristics between neutrons and gamma rays when they penetrate the plastic scintillator, the ratios of the slow component's charge to the total charge are different for the pulse signals of neutrons and gamma rays. Based on the aforementioned characteristics, Hawkes et al. calculated the charge ratio R to discriminate n-γ signals [32], defined as follows:

$$R = \frac{Q_{\mathrm{N}}}{Q_{\mathrm{M}}}, \tag{13}$$

where Q_{N} and Q_{M} represent the summations of the pulse voltage of the slow component and the whole signal, respectively. As a result of the longer decay time and delayed fluorescence of neutrons, the R-value is larger than that of gamma rays.

2.5 Filtering methods

Inevitably, the pulse signals detected by the radiation detector always incorporate noise, which makes the difference between the pulse signals of neutrons and gamma rays much less significant. Thus, the performance of direct n-γ discrimination is affected by the useless noise, making the preprocessing of the pulse signals especially important. There are many preprocessing methods, also called filtering methods, which are commonly used in radiation detection, such as the Fourier transform [33–35], wavelet transform [36–38], Kalman filter [39], and sliding average filter [40]. A discrimination method shows different discrimination effects with different filtering methods; we have demonstrated in our previous work [17] that each discrimination method has the best-matched filtering method, with which it can achieve optimized performance.

In the present work, the discussion mainly regards the performance of different discrimination methods; hence, only one is uniformly used as the filtering method for all discrimination methods. In this work, the Fourier transform is selected as the filtering method due to its generally good performance when coupled with most discrimination methods [17] and its common application in radiation detection.

After implementing the Fourier transform, the pulse signal is transformed from the time-domain to the frequency-domain, where the low-amplitude frequency-domain information is the noise component. Filtering is realized by removing the noise component in the frequency-domain and further taking the inverse Fourier transform to obtain the pulse signal back to the time-domain. As a result of the discrete sampling process being required when the pulse signals are retrieved from the n-γ superposed field, the pulse signals are discrete; hence, a discrete Fourier transform (DFT) is required to filter the n-γ pulse signals. The mathematical transform formulas are as follows:

$$\boldsymbol{G}(u) = \sum_{x=1}^{N} \boldsymbol{g}(x) e^{-i\frac{2\pi}{N}xu} = \sum_{x=1}^{N} \boldsymbol{g}(x)\omega_N^{xu} (x = 1, 2, \ldots, N), \tag{14}$$

$$\boldsymbol{g}(x) = \frac{1}{N}\sum_{x=1}^{N} \boldsymbol{G}(u) e^{i\frac{2\pi}{N}xu} = \frac{1}{N}\sum_{x=1}^{N} \boldsymbol{G}(u)\omega_N^{-xu} (x = 1, 2, \ldots, N), \tag{15}$$

where Eq. (14) is the positive transform formula for the DFT, Eq. (15) is the inverse transform formula for the DFT, $\omega_N = e^{(-2\pi i)/N}$ denotes the frequency, $\boldsymbol{G}(u)$ represents the frequency-domain signal, $\boldsymbol{g}(x)$ denotes the time-domain signal, and N is the length of a signal.

3 Evaluation criteria

To evaluate the performance of different n-γ discrimination methods, objective evaluation criteria need to be used, which are the discrimination time (the CPU time required to process all given pulse signals) and the figure of merit (FoM) in this work. Regarding calculation of the FoM-value, the histogram of counts of neutrons and gamma rays must be drawn after the discrimination process, as shown in Fig. 2. Then, the mathematical formula of FoM [41] is given as follows:

$$FoM = \frac{S}{FWHM_{\mathrm{n}} + FWHM_{\gamma}} \tag{16}$$

where S denotes the distance between the neutron count and gamma ray count peaks, $FWHM_{\mathrm{n}}$ and $FWHM_{\gamma}$ are the

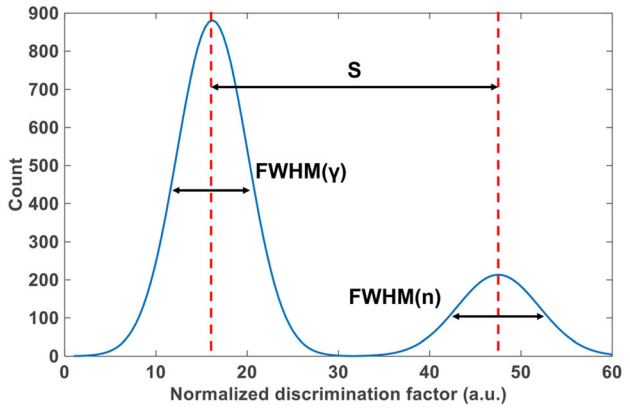

Fig. 2 (Color online) n-γ discrimination evaluation criteria. The evaluation criteria *FoM*-value is defined by Eq. (14), incorporating three parts that are marked in this figure (S, $\mathrm{FWHM_n}$, and FWHM_γ). A greater *FoM*-value corresponds to a better discrimination effect

half-height widths of the neutron counting peak and gamma ray counting peak, respectively, estimated by Gaussian fitting. A larger *FoM*-value corresponds to a better discrimination effect.

4 Experiment

4.1 Parameter settings

4.1.1 PCNN

The parameters of the PCNN are set as: $n = 180$, $\alpha_\mathrm{F} = 0.32$, $\alpha_\mathrm{L} = 0.356$, $\alpha_\theta = 0.08$, $V_\mathrm{F} = 0.0005$, $V_\mathrm{L} = 0.0005$, $V_\theta = 15$, and linking weight $\boldsymbol{M} = [0.1409, 0, 0.1409]$. The n-$\gamma$ signals processed by the PCNN using the aforementioned parameters are shown in Fig. 3b. The ignition maps of pulse signals between 10 ns before the peak and 20 ns after the peak were selected as the discrimination intervals.

4.1.2 Other methods

To train the BPNN, 11,454 well-discriminated and low-noise signals were selected as the training set. There are two hidden layers of the BPNN used in our work, each of which has nine neurons. The entire training process took approximately 0.2 s, which is included in the total time consumption of BPNN in Table 1. With regard to the fractal spectrum method, the pulse signals from 38 to 130 ns after the peak were chosen as the discrimination interval. In the charge comparison method, the total component is composed of pulse signals between 15 ns before the peak and 200 ns after the peak and the slow component incorporates pulse signals between T and 200 ns after the peak. T is delay time, i.e., a parameter between 155 and 185 ns that affects the *FoM*-value of the charge comparison method. The abovementioned parameters of these three methods were optimized in our previous work [17].

4.2 Experimental results and discussions

4.2.1 Pulse signals of neutrons and gamma rays

In this work, a ^{241}Am-Be isotope neutron source was used to generate the n-γ superposed field, with an average energy of 4.5 MeV. The detection equipment was composed of two parts: an EJ299-33 plastic scintillator and a digital oscilloscope with a 500 mV trigger threshold (which corresponds to an energy of approximately 1.6 MeVee, where 1 MeVee (i.e., MeV electron equivalent) is defined as the amount of energy converted to light induced by an electron, which deposits 1 MeV in the scintillator), a 200 MHz bandwidth, and a 1 GS/s sampling rate. Based on this setup, 9414 pulse signals were retrieved. A comparison of the normalized neutron and gamma ray signals that we retrieved is shown in Fig. 3a. It can be seen that the rise speeds of both signals are similar, while the luminous attenuation rate of the neutron is noticeably slower than that of gamma rays; this is attributed to its longer decay time and delayed fluorescence [42].

4.2.2 Discrimination results

The 9414 n-γ pulse signals were filtered by the Fourier transform [34] and then discriminated by the aforementioned methods (processed on an AMD R9-5900X CPU); the results are shown in Figs. 4, 5.

Figure 4 shows the scatter plot of pulse signals discriminated by different methods, where the dots above the crossing line are discriminated as neutron signals and the dots below the crossing line are discriminated as gamma ray signals. For a good discrimination result, the group of neutron dots and the group of gamma ray dots should be separated and each group should be distributed as centrally as possible while maintaining a good Gaussian distribution at the same time. It can be clearly seen that the PCNN method noticeably outperforms the others, with a clear gap between the neutron and gamma ray dots. Meanwhile, both groups were centrally distributed, with very few dots located between the two groups or discrete on the outer sides.

Figure 5 shows the Gaussian fitting of the histogram of the four methods. The discrimination effect is reflected in two aspects: (i) the length of the gap between the two peaks and (ii) the shape of the two peaks. A wider gap corresponds to better discrimination. The narrower and higher neutron peak (on the right side) and gamma peak (on the

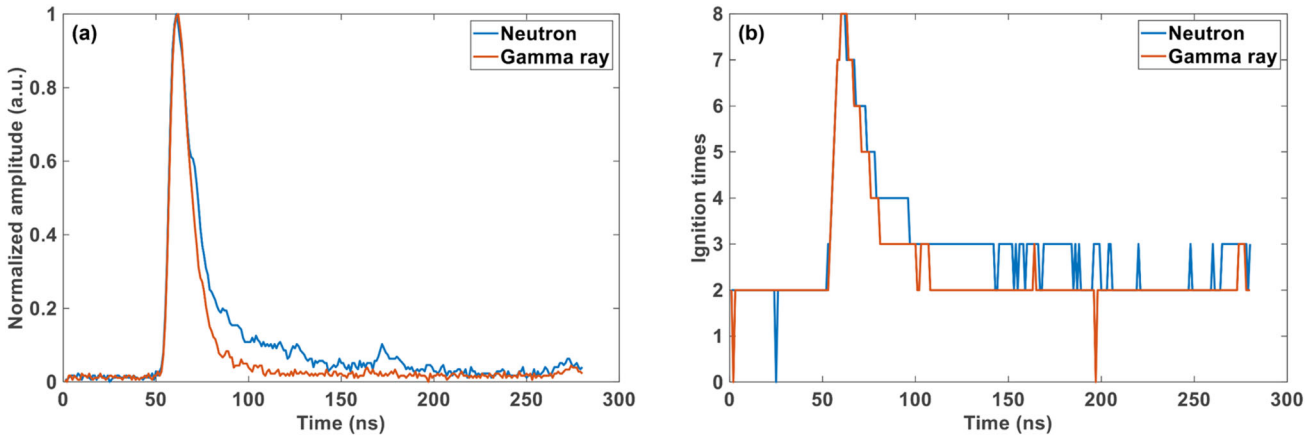

Fig. 3 (Color online) Comparison of normalized n–γ pulses and their ignition maps. **a** The pulse signals of neutron and gamma ray. **b** The ignition maps of neutron and gamma ray, which are obtained by implementing PCNN on n–γ pulse signals. The difference between neutron and gamma ray in (b) is similar but more distinct than that in (a), demonstrating that the inherent differences between n–γ pulses are successfully detected by the PCNN

Table 1 Discrimination time and *FoM* value of different discrimination methods

Discrimination method	Charge comparison	BPNN	Fractal spectrum	PCNN
Discrimination time	1.96 s	3.65 s	178.01 s	2.22 s
Discrimination effect (*FoM*)	1.351	0.989	1.028	1.709

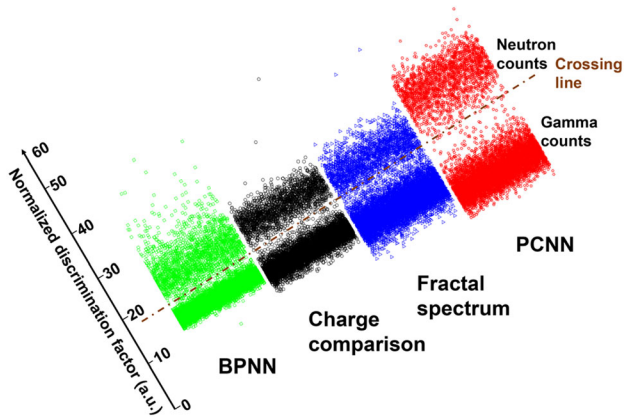

Fig. 4 (Color online) Scatter plot of pulse signals discriminated by different methods. The dots above the crossing line are discriminated as neutron signals and the dots below the crossing line are discriminated as gamma ray signals. Well-separated neutron dots and gamma ray dots indicate a good discrimination effect

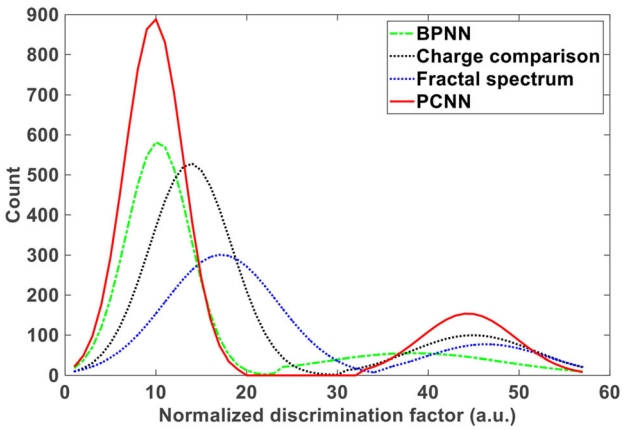

Fig. 5 (Color online) Gauss fitting curves for the histogram of four discrimination methods. A longer distance between neutrons and gamma ray counting peaks or narrower and higher n–γ counting peaks indicates a better discrimination performance

left side) represent better discrimination performance. As shown in Fig. 5, the fitting curve of the PCNN method exhibits better performance than that of the other methods, with a longer distance between neutrons and gamma ray counting peaks and has narrower and higher n-γ counting peaks.

To quantitatively evaluate the performance of these methods, the *FoM*-value of their discrimination results were calculated, as presented in Table 1, along with the discrimination time (for the processing time of the 9414 pulse signals) of each method.

Table 1 demonstrates that our proposed method significantly outperforms the others, with a 26.49% improvement in the FoM-value compared to the charge comparison method, a 72.80% improvement compared to the BPNN, and a 66.24% improvement compared to the fractal spectrum method. This outstanding discrimination performance of the proposed method is because the PCNN is not based on every single point of a fixed vector of the input signal, as in other methods. In contrast, the PCNN not only

considers the amplitude of a point but also the amplitudes of points before and after this location, i.e., the PCNN treats the input signal as a whole for analysis and processing, imparting an excellent anti-noise effect and the ability to process the dynamic information contained in a pulse signal. In addition, the discrimination time of our proposed method is quite satisfactory (2.22 s), taking slightly longer than the charge comparison method (1.96 s) and outperforming the BPNN (3.65 s) and fractal spectrum method (178.01 s). As a neural network, the PCNN takes such a short time compared to the BPNN and the fractal spectrum is attributed to its simple computational complexity, with fewer matrix operations compared to the fractal spectrum and without the need for a pre-training step compared to the BPNN. This experimental result shows that the PCNN has the potential to be implemented in real-time applications.

5 Conclusion

In this work, a PCNN-based n-γ discrimination method is proposed and compared with the other three methods, including the BPNN, fractal spectrum method, and charge comparison method. Our experiment was conducted on the data of an EJ299-33 plastic scintillator, by which 9414 n-γ pulse signals were retrieved and further processed on an AMD R9-5900X CPU. The experimental results show that our proposed method significantly outperforms the others, with the best *FoM*-value and short discrimination time. Specifically, the PCNN demonstrates a 26.49% improvement in the *FoM*-value compared to the charge comparison method, a 72.80% improvement compared to the BPNN, a 66.24% improvement compared to the fractal spectrum method, and the second-fastest discrimination time of 2.22 s. This outstanding performance is because the PCNN treats the input signal as a whole for analysis and processing, imparting an excellent anti-noise effect and the ability to process the dynamic information contained in a pulse signal. This short discrimination time of the PCNN is due to its simple computational complexity, with few matrix operations and without the need for a pre-training step. The distinguished n-γ discrimination effect of the PCNN enables broad application prospects in the radiation detection field and its relatively short discrimination time makes it potentially useful for real-time discrimination. To the best of our knowledge, this is the first report on applying a pulse-coupled neural network for n-γ discrimination. In our future work, we will verify the feasibility of other improved PCNN models, aiming to achieve an even better discrimination effect and shorter discrimination time.

Author contributions All authors contributed to the study conception and design. Material preparation, data collection, and analysis were performed by Hao-Ran Liu, Yu-Xin Cheng, Zhuo Zuo, Tian-Tian Sun, and Kai-Min Wang. The first draft of the manuscript was written by Hao-Ran Liu, and all authors commented on previous versions of the manuscript. All authors read and approved the final manuscript.

References

1. D.D. Zhou, S.M. You, J. Xin et al., Development of a 4π phoswich detector for measuring radioactive inert gases. Nucl. Tech. 43, 050401 (2020). Doi: https://doi.org/10.11889/j.0253-3219.2020.hjs.43.050401 (in Chinese)
2. X. Zhang, X. Yuan, X.F. Xie et al., A digital delay-line-shaping method for pulse shape discrimination in stilbene neutron detector and application to fusion neutron measurement at HL-2A tokamak. Nucl. Instrum. Meth. Phys. A **687**, 7–13 (2012). https://doi.org/10.1016/j.nima.2012.05.077
3. Y. Sun, G.L. Liu, X.L. Luo, Near space neutron environment and detection. Natl. Def. Sci. Technol. **35**, 24–28 (2014). https://doi.org/10.3969/j.issn.1671-4547.2014.01.007 (in Chinese)
4. M.P. Blakeley, S.C.M. Teixeira, I. Petit-Haertlein et al., Neutron macromolecular crystallography with LADI-III. Acta Cryst. D **66**, 1198–1205 (2010). https://doi.org/10.1107/S0907444910019797
5. A. El-Taher, Rare earth elements content in geological samples from eastern desert, Egypt, determined by instrumental neutron activation analysis. Appl. Radiat. Isotopes **68**(9), 1859–1863 (2010). https://doi.org/10.1016/j.apradiso.2010.02.012
6. G. Tosi, A. Torresin, S. Agosteo et al., Neutron measurements around medical electron accelerators by active and passive detection techniques. Med. Phys. **18**(1), 54 (1991). https://doi.org/10.1118/1.596751
7. W.J. Guo, X.M. Wu, J. Wang, Preliminary study of neutron (waterice) detector on moon and mars. Spacecr. Eng. **19**(05), 64–69 (2010)
8. F.D. Brooks, Development of organic scintillators. Nucl. Instrum. Methods **162**(1–3), 477–505 (1979). https://doi.org/10.1016/0029-554X(79)90729-8
9. D. Cester, M. Lunardon, G. Nebbia et al., Pulse shape discrimination with fast digitizers. Nucl. Instrum. Meth. Phys. A **748**, 33–38 (2014). https://doi.org/10.1016/j.nima.2014.02.032
10. M.L. Roush, M.A. Wilson, W.F. Hornyak, Pulse shape discrimination. Nucl. Instrum. Methods **31**(1), 112–124 (1964). https://doi.org/10.1016/0029-554X(64)90333-7
11. C. Frangville, A. Grabowski, J. Dumazert et al., Nanoparticles-loaded plastic scintillators for fast/thermal neutrons/gamma discrimination: simulation and results. Nucl. Instrum. Meth. Phys. A **942**, 162370 (2019). https://doi.org/10.1016/j.nima.2019.162370
12. R. Coulon, V. Kondrasovs, Q. Lecomte et al., Multilayer phoswich scintillators for neutron/gamma discrimination. Radiat. Meas. **117**, 57–62 (2018). https://doi.org/10.1016/j.radmeas.2018.07.011
13. F.D. Brooks, R.W. Pringle, B.L. Funt, Pulse shape discrimination in a plastic scintillator. IRE T. Nucl. Sci. **7**, 35–38 (1960). https://doi.org/10.1109/TNS2.1960.4315733
14. P. Blanc, M. Hamel, L. Rocha et al., Study and understanding of n/γ discrimination in organic plastic scintillators. In: 2012 *IEEE Nuclear Science Symposium and Medical Imaging Conference Record (NSS/MIC)*, 1978–1982 (2012). https://doi.org/10.1109/nssmic.2012.6551457
15. N. Zaitseva, B.L. Rupert, I. PaweŁczak et al., Plastic scintillators with efficient neutron/gamma pulse shape discrimination. Nucl.

Instrum. Meth. Phys. A **668**, 88–93 (2012). https://doi.org/10.1016/j.nima.2011.11.071
16. M.Z. Liu, B.Q. Liu, Z. Zuo et al., Toward a fractal spectrum approach for neutron and gamma pulse shape discrimination. Chin. Phys. C **40**, 066201 (2016). https://doi.org/10.1088/1674-1137/40/6/066201
17. Z. Zuo, H.R. Liu, Y.C. Yan et al., Adaptability of n–γ discrimination and filtering methods based on plastic scintillation. Nucl. Sci. Tech. **32**, 28 (2021). https://doi.org/10.1007/s41365-021-00865-3
18. C.X. Zhang, S.T. Lin, J.L. Zhao et al., Discrimination of neutrons and γ-rays in liquid scintillator based on Elman neural network. Chin. Phys. C **40**(8), 086204 (2016). https://doi.org/10.1088/1674-1137/40/8/086204
19. J. Iwanowska-Hanke, M. Moszynski, L. Swiderski et al., Comparative study of large samples (2“ × 2”) plastic scintillators and EJ309 liquid with pulse shape discrimination (PSD) capabilities. J. Instrum. **9**(6), P06014 (2014). https://doi.org/10.1088/1748-0221/9/06/P06014
20. R. Eckhorn, H.J. Reitboeck, M. Arndt et al., Feature linking via synchronization among distributed assemblies: simulations of results from cat visual cortex. Neural Comput. **2**(3), 293–307 (1990). https://doi.org/10.1162/neco.1990.2.3.293
21. R. Eckhorn, H.J. Reitbock, M. Arndt et al., A neural network for feature linking via synchronous activity: Results from cat visual cortex and from simulations. In: Rodney M. J. Cotterill (ed.), Models of Brain Function, Cambridge University Press, pp. 255–272 (1989). https://philpapers.org/rec/ECKANN
22. C.M. Gray, W. Singer, Stimulus-specific neuronal oscillations in orientation columns of cat visual cortex. P. Natl. Acad. Sci. USA **86**(5), 1698–1702 (1989). https://doi.org/10.1073/pnas.86.5.1698
23. H.J. Reitboeck, R. Eckhorn, M. Arndt et al., A model of feature linking via correlated neural activity, in *Synergetics of Cognition*, vol. 45, ed. by H. Haken, M. Stadler (Springer, Berlin Heidelberg, 1990)
24. H.S. Ranganath, G. Kuntimad, J.L. Johnson, Pulse coupled neural networks for image processing. Proceedings IEEE Southeastcon ’95. Visualize the Future, 1995, pp. 37–43, https://doi.org/10.1109/SECON.1995.513053
25. J.L. Johnson, M.L. Padgett, PCNN models and applications. IEEE T. Neural Netw. **10**(3), 480–498 (1999). https://doi.org/10.1109/72.761706
26. J. L. Johnson, H. Ranganath, G. Kuntimad et al, Pulse-coupled neural networks. In: O. Omidvar and J. Dayhoff (Eds) Neural Networks and Pattern Recognition. San Diego, CA: Academic (1998). https://doi.org/10.1016/B978-012526420-4/50002-1
27. A.T.C. Goh, Back-propagation neural networks for modeling complex systems. Artif. Intell. Eng. **9**, 143–151 (1995). https://doi.org/10.1016/0954-1810(94)00011-S
28. K. Hornik, Approximation capabilities of multilayer feedforward networks. Neural Netw. **4**(2), 251–257 (1991). https://doi.org/10.1016/0893-6080(91)90009-t
29. B. Esposito, L. Fortuno, A. Rizo, Neural neutron/gamma discrimination in organic scintillators for fusion applications. In: Proceedings of the 2004 IEEE International Joint Conference on Neural Networks, Budapest, Hungary, 2004, vol. 4, pp. 2931–2936 (2004). https://doi.org/10.1109/IJCNN.2004.1381130
30. E. Ronchi, P.A. Soderstrom, J. Nyberg et al., An artificial neural network based neutron-gamma discrimination and pile-up rejection framework for the BC-501 scintillation detector. Nucl. Instrum. Meth. Phys. A **610**, 534–539 (2009). https://doi.org/10.1016/j.nima.2009.08.064
31. D. Wolski, M. Moszyński, T. Ludziejewski et al., Comparison of n-γ discrimination by zero-crossing and digital charge comparison methods. Nucl. Instrum. Methds Phys. Res. Sect. A Accel. Spectrom. Detect Assoc. Equip. **360**(3), 584–592 (1995). https://doi.org/10.1016/0168-9002(95)00037-2
32. N.P. Hawkes, K.A.A. Gamage, G.C. Taylor, Digital approaches to field neutron spectrometry. Radiat. Meas. **45**(10), 1305–1308 (2010). https://doi.org/10.1016/j.radmeas.2010.06.043
33. K. Yang, P.R. Menge, V. Ouspenski, Enhanced α-γ discrimination in co-doped LaBr3:Ce, In: 2014 IEEE Nuclear Science Symposium and Medical Imaging Conference (NSS/MIC), 2014, pp. 1–5 (2014). https://doi.org/10.1109/NSSMIC.2014.7431223
34. J. Allem, Short term spectral analysis, synthesis, and modification by discrete Fourier transform. IEEE Trans. Acoust. **25**(3), 235–238 (1997). https://doi.org/10.1109/TASSP.1977.1162950
35. T.G. Payne, A.D. Southam, T.N. Arvanitis et al., A signal filtering method for improved quantification and noise discrimination in Fourier transform ion cyclotron resonance mass spectrometry-based metabolomics data. J. Am. Soc. Mass Spectrom. **20**, 1087–1095 (2009). https://doi.org/10.1016/j.jasms.2009.02.001
36. S. Yousefi, L. Lucchese, M.D. Aspinall, Digital discrimination of neutrons and gamma-rays in liquid scintillators using wavelets. Nucl. Instrum. Meth. A **598**, 551–555 (2009). https://doi.org/10.1016/j.nima.2008.09.028
37. S. Hosur, A.H. Tewfik, Wavelet transform domain adaptive FIR filtering. IEEE Trans. Signal Process. **45**, 617–630 (1997). https://doi.org/10.1109/78.558477
38. H. Singh, R. Mehra, Discrete wavelet transform method for high flux n-c discrimination with liquid scintillators. IEEE Trans. Nucl. Sci. **64**, 1–7 (2017). https://doi.org/10.1109/TNS.2017.2708602
39. J.A. Burns, E.M. Cliff, C. Rautenberg, A distributed parameter control approach to optimal filtering and smoothing with mobile sensor networks. In: 2009 17th Mediterranean Conference on Control and Automation, 2009, pp.181–186. https://doi.org/10.1109/MED.2009.5164536
40. Y. Zheng, S. Chen, W. Tan et al., Detection of tissue harmonic motion induced by ultrasonic radiation force using pulse-echo ultrasound and a Kalman filter. IEEE Trans. Ultrason. Ferroelectr. Freq. Control **54**, 290–300 (2007). https://doi.org/10.1109/TUFFC.2007.243
41. R.A. Winyard, J.E. Lutkin, G.W. McBeth, Pulse shape discrimination in inorganic and organic scintillators. I. Nucl. Instrum. Meth. **95**(1), 141–153 (1971). https://doi.org/10.1016/0029-554X(71)90054-1
42. B. D’Mellow, M.D. Aspinall, R.O. Mackin et al., Digital discrimination of neutrons and γ-rays in liquid scintillators using pulse gradient analysis. Nucl. Instrum. Meth. Phys. A **578**(1), 191–197 (2007). https://doi.org/10.1016/j.nima.2007.04.174